Asian Journal of Chemistry; Vol. 36, No. 2 (2024), 481-488

ASIAN JOURNAL OF CHEMISTRY

https://doi.org/10.14233/ajchem.2024.31153

Metal Organic Framework Derived Cu-Carbon Composite for the Effective Reduction of *p*-Nitrophenol

ZUBAIR HASAN[1,*], MD. SHARIFUL ISLAM[2], MAHMUD HASSAN[1], MD. NAZMUL ABEDIN KHAN[1], MOHAMMAD MAHBUBUR RAHMAN[3] and MOHAMMAD FARHADUR RAHMAN[4,*]

[1]Department of Mathematical and Physical Sciences, East West University, Dhaka, Bangladesh
[2]Department of Pharmacy, East West University, Dhaka, Dhaka, Bangladesh
[3]Fiber & Polymer Research Division, BCSIR Laboratories, Dhaka, Bangladesh
[4]Department of Chemistry, Bangladesh University of Textiles, Dhaka, Bangladesh

*Corresponding author: E-mail: zhasan@ewubd.edu; chemistry.butex2010@gmail.com

Received: 5 November 2023; *Accepted*: 18 January 2024; *Published online*: 31 January 2024; AJC-21537

A Cu-carbon composite (Cu-C) was prepared *via* single-step carbonization of a metal-organic framework (MOF) composed of Cu^{2+} and 1,4-benzene dicarboxylate (BDC) and applied as a catalyst to degrade *p*-nitrophenol. The composite was characterized by X-ray powder diffraction (XRD), scanning electron microscope (SEM)/energy-dispersive X-ray (EDS), Fourier-transform infrared (FTIR) and X-ray photoelectron (XPS) spectroscopies. The characterization affirmed the preservation of MOF-originated CuO and metallic Cu in the carbon network. In presence of $NaBH_4$, the Cu-C composite resulted in a complete reduction of *p*-nitrophenol within a few min and exhibited much higher removal rate than commercial CuO. The role of $NaBH_4$ concentration in *p*-nitrophenol reduction was highlighted in the context of relevant catalytic mechanisms. The composite displayed good reusability during four consecutive cycles of *p*-nitrophenol reduction with only a small loss of its reactivity, signifying its potential as an alternative to noble-metal catalysts.

Keywords: Metal-organic framework, *p*-Nitrophenol, Reduction, Metallic copper.

INTRODUCTION

Nitrophenols are persistent organic pollutants generated as a byproduct of various industrial processes such as pesticide manufacturing, petroleum refining, plasticizers production, dyes manufacturing, pharmaceutical industries, *etc*. [1-3]. Because of their widespread occurrence and detrimental impacts on the ecosystem, nitrophenols are included in the list of "Priority Pollutants" of the United States Environmental Protection Agency (USEPA), with their regulatory limit set at 10 ng L^{-1} in natural waterways [4]. Among three mono-substituted nitrophenols, 4-nitrophenol has received the most attention for its wide occurrence and adverse health effects on humans, as it causes respiratory problems, blood disorders, skin irritation and carcinogenic and mutagenic effects [2]. *p*-Nitrophenol is very soluble in water and has high bioavailability [5]. Hence, the presence of *p*-nitrophenol in water resources is considered a serious environmental threat to aquatic and human life.

To address the *p*-nitrophenol pollution in aquatic environments, several techniques have been suggested for removal of *p*-nitrophenol, including catalytic [6] or photocatalytic degradation [7], adsorption [8], microbial degradation [9], electrocoagulation and electro-Fenton method [10], *etc*. Conventional aquatic pollutant removal methods can be classified into two types for example, (i) those aiming for permanent removal of target pollutants and (ii) those aiming for converting target pollutants into useable or non-toxic forms. The catalytic reduction of *p*-nitrophenol utilizing redox-active catalytic materials is relevant to the latter case as it catalytically converts *p*-nitrophenol into *p*-aminophenol, which can be reclaimed as a source chemical in the production of various pharmaceuticals [10]. In this sense, catalytic conversion is a desirable and beneficial option for treating *p*-nitrophenol.

Several noble metals such as Au, Ag and Pd have been extensively examined for the catalytic reduction of organic pollutants in aquatic media. However, the high cost of noble

metals has prohibited large-scale commercial applications and prompted researchers to investigate the potential utility of non-noble metal catalysts, including Cu, Co, Ni, Zn, *etc.* [11-13]. Nonetheless, single-component non-noble metal catalysts are reported to be structurally unstable and prone to agglomeration, which adversely influences the activity and longevity of the catalysts [14]. For this reason, exploration to find stable catalyst is still in search [15]. For example, Cu_2O and CuO oxides are easily synthesized from Cu salts or metals. Between them, the latter is more stable due to less oxidative properties and considered an efficient and non-toxic material that finds many field applications as heterogeneous catalysts or adsorbents [15]. Moreover, metal oxides including CuO are often combined with solid supports to further improve catalytic reactions [16]. For instance, collective assemblies of composite materials comprising active metal/metal oxides homogeneously dispersed on solid supports such as carbon [17], biochar [16] and silica [18] have been demonstrated to exhibit more efficient catalytic reactions in a wide range of applications.

Metal organic frameworks (MOFs) are an intriguing class of porous solids possessing several advantageous properties as an environmental treatment medium [19,20]. These include high surface area and porosity, adjustable pore structure and specific functionalities arising from unique carbon framework and central metallic components. Because of these features, MOFs have been utilized in several environmental applications, including adsorption [21,22], gas storage/separation [23], fuel purification [24], catalysis [25], sensing [26], *etc.* In addition, MOFs were used as templates for synthesizing porous carbonaceous solids [27]. Wang *et al.* [28] used MOF-5 as a template to synthesize highly porous carbonaceous material with adjustable pore sizes. On the other hand, direct carbonization of MOFs was also reported to prepare MOF-derived metal carbon composites [29]. These metal carbon composites exhibited good activity as catalysts or absorbents.

In this study, a Cu-based MOF, Cu-BDC (1,4-benzene dicarboxylic acid, BDC as organic linker), was synthesized hydrothermally. The synthesized MOF was carbonized under an inert atmosphere to prepare Cu-carbon (Cu-C) composite and characterized using various analytical instruments and further applied as catalyst to $NaBH_4$-assisted reduction of *p*-nitrophenol. The catalytic performance of the composites was assessed by conducting a series of experiments, including the effects of $NaBH_4$ concentration, kinetics and reusability.

EXPERIMENTAL

All the chemicals used in this study were obtained from commercial suppliers and used without further purification. Copper(II) nitrate pentahydrate [$Cu(NO_3)_2{\cdot}5H_2O$], benzene-1,4-dicarboxylic acid (H_2BTC, 97%) and *N*,*N*-dimethylformamide (99.5%) were purchased from Sigma-Aldrich, USA. Sodium borohydride ($NaBH_4$), methanol (99.5%), ethanol (99.9%), hydrochloric acid (37%), Activated carbon were purchased from Daejung chemicals, South Korea.

Synthesis of Cu-BDC: For the synthesis of Cu-BDC, 1.12 g $Cu(NO_3){\cdot}5HO_2$ (4.8 mmol) and 0.8 g H_2BDC (4.8 mmol) were taken into a 100 mL beaker. A 60 mL of DMF was added to dissolve the reagents and the mixture was sonicated at 25 ºC for 30 min. Then, the mixture was poured into a 100 mL Teflon-lined autoclave vessel and preheated conventional electric oven at 110 ºC for 24 h. When the reaction was complete, the vessel was cooled to room temperature and blue-coloured solid products were recovered *via* filtration. The as-synthesized Cu-BDC contained unreacted BDC, which was removed by washing with DMF and ethanol, followed by drying overnight at 100 ºC and storing in a desiccator before use.

Synthesis of MOF-derived carbon catalyst: The prepared Cu-BDC was further calcined to produce the carbon composite. A 1.5 g Cu-BDC was taken into an alumina tube (700 mm long, 40 mm width), placed in the split-hinged tube furnace (SK2-5-14TB3, China) and heated at 600 ºC under N_2 atmosphere for 3 h. The N_2 gas flow rate was fixed at 300 mL min^{-1} with an acrylic flow meter. After cooling to room temperature, a black powder was obtained. All the products were washed thoroughly with ethanol and water to remove unwanted organic and inorganic moieties. After washing, the composite was dried and stored for subsequent use and denoted as Cu-C.

Characterization: X-ray powder diffraction (XRD) analysis was carried out using a Rigaku DMax-2500 diffractometer having Cu*K*α radiation. The morphologies and composition of the samples were examined with field emission scanning electron microscopy (FE-SEM, JEOL-JSM7401F) coupled with energy dispersive X-ray spectroscopy (EDX). The Fourier-transform infrared spectroscopy (FTIR) analysis was recorded in transmittance mode on a Shimadzu spectrophotometer in the 4000-650 cm^{-1} range. X-ray photoelectron spectroscopy (XPS) and Auger electron spectroscopy (AES) experiments were conducted using a K-Alpha XPS System (Thermofisher). A Shimadzu UV-1900 (Japan) spectrophotometer was used to measure the catalytic reduction of textile dyes in the wavelength range of 200-700 nm.

Reduction of *p*-nitrophenol: Reduction of *p*-nitrophenol was conducted using $NaBH_4$ as bulk reductant. The reaction was carried out in a conventional quartz cuvette with a 1 cm path length at room temperature. The response was monitored using a UV-visible spectrophotometer (Shimadzu-1900, Japan). For every batch reaction, freshly prepared $NaBH_4$ was used. At first, the cuvette was charged with 0.2 mL of 2.5 mM *p*-nitrophenol and 2.5 mL deionized water. Then, 0.2 mL of aqueous dispersion of the prepared composite (1 mg mL^{-1}) was added. The reaction was initiated by adding 0.2 mL $NaBH_4$ solution, which immediately changed from pale yellow to bright yellow. The mixture was directly introduced to a UV-vis spectrophotometer for *p*-nitrophenol analysis. The kinetics data of *p*-nitrophenol reduction were obtained by monitoring the absorbance at 400 nm.

RESULTS AND DISCUSSION

Characterization: The XRD pattern (Fig. 1a) of Cu-BDC exhibited close agreement with the simulated XRD pattern, which confirmed the successful synthesis of desired precursor. Fig. 1b revealed that the main mineralogical phases in Cu-BDC disappeared and new diffraction peaks corresponding to Cu and CuO phases evolved. The peaks at 2θ values of 35.7º and 38.9º could be attributed to the (002) and (111) facets of CuO,

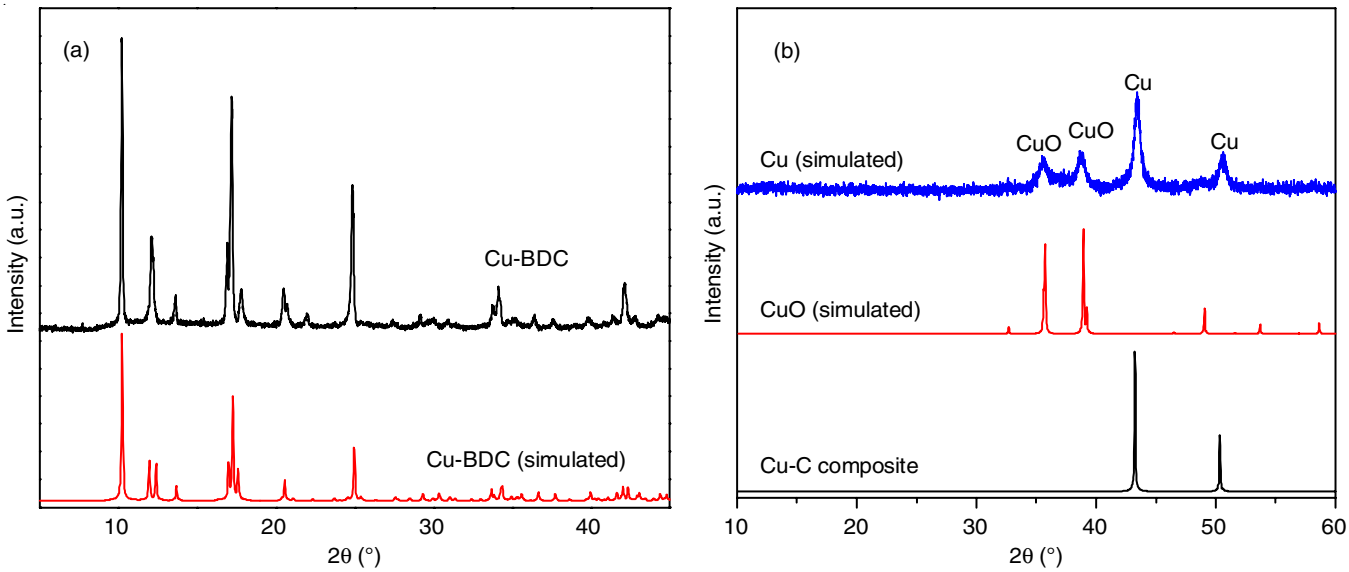

Fig. 1. (a) XRD patterns of Cu-BDC and (b) Cu-C composites

respectively [30]. In addition, peaks at 43.34° and 50.23° could be ascribed to the (111) and (220) facets of metallic Cu, respectively [31].

The FTIR spectra of Cu-BDC and Cu-C are shown in Fig. 2. The weak and narrow bands at 1018 and 750 cm^{-1} can be attributed to δ(C–H) and γ(C–H) vibration of aromatic rings, respectively [32], which signifies the presence of the organic ligand (linker) in Cu-C. The bands at 1505 cm^{-1} belong to vibrations of the phenyl ring [32]. The strong absorption at 1670 cm^{-1} corresponds to carbonyl C=O groups. The peak at 1387 cm^{-1} is attributed to the stretching of C-O that is shifted towards the lower absorption band. The peaks at 1425 and 1506 cm^{-1} are due to the absorbance of C=C stretching of the aromatic ring in the linker [33]. The FTIR spectrum of Cu-C shows several vibration bonds of Cu oxides below 1000 cm^{-1} [34]. The peaks at 600 and 610 cm^{-1} can be attributed to Cu–O stretching vibrations. The presence of carbon moieties is evinced by the peaks at 1110 and 1636 cm^{-1}, which correspond to C–O and C=O stretching, respectively [34]. The broad peak near 3452 cm^{-1} corresponds to the O–H stretching vibration modes [31].

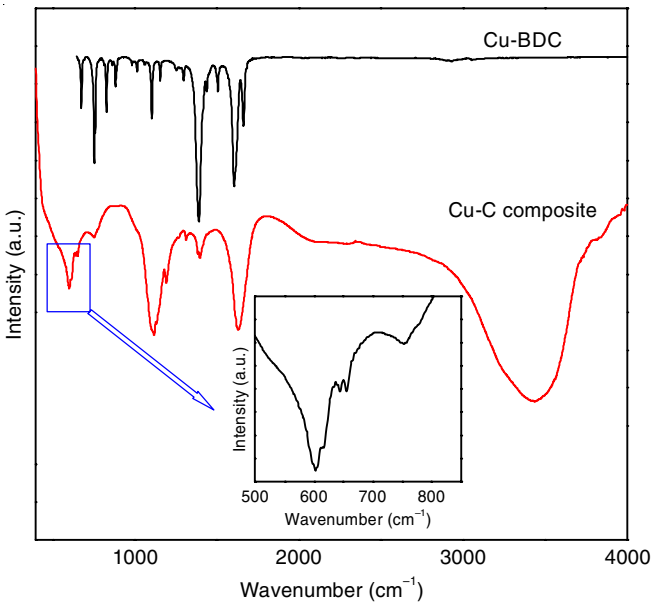

Fig. 2. FTIR spectra of Cu-BDC and Cu-C composites

Fig. 3 shows the surface morphology of Cu-BDC and Cu-C at 15000X magnification. The Cu-BDC particles are arranged irregularly, having sizes ranging from 1 to 8 μm with ill-defined shapes (Fig. 3a). The image of Cu-C shows particulate matters with reduced particle size as compared to Cu-BDC (Fig. 3b). The particles are agglomerated and irregularly arranged, having no definitive shape and size ranging from 200 nm to 1 μm. Moreover, EDX analysis of Cu-C confirmed the presence of carbon, oxygen and copper as the main components.

To further understand the surface composition of Cu-C, high-resolution XPS and Auger CuLM2 spectra analyses were conducted and results are presented in Fig. 4. Since different oxidation states of Cu (0, +I and +II) tend to exhibit close binding energies, the sole use of Cu 2p spectrum does not provide clear cut evidence to distinguish the oxidation states of Cu embedded on carbon matrix [35]. To overcome this problem, the Auger CuLM2 spectra were employed, along with analysis of shakeup satellite peaks [35]. Fig. 4 represents the deconvoluted Cu2p spectrum of Cu-C without Ar etching. The Cu2p depth profiles show two vital peaks at 932.9 and 952.8 eV, which could be ascribed to the $Cu2p_{3/2}$ and $Cu2p_{1/2}$ spin–orbit peaks of Cu^{2+}, respectively [36]. Furthermore, two firm satellite peaks near 940 and 962 eV (Fig. 4a) also indicate the presence of a Cu(+II) oxidation state [36]. Nevertheless, the CuLM2 peaks occurred at 917.4 eV (Fig. 4b), which further confirmed the presence of Cu(+II) phase [35]. However, when the XPS spectra were taken after two consecutive Ar etchings, the peak evolved at 916.8 eV (Fig. 4c), revealing the presence of Cu(+I) beneath the surface [35]. Although the XRD confirmed the existence of metallic Cu, the CuLM2 peaks did not identify Cu(0) at deeper layers of Cu-C. Fig. 4d is deconvoluted C1s scan that clearly shows very large peaks of C=C/C-C (284.8 eV) along with small peaks pertaining to C-O/C-O-C (286.2 eV) and

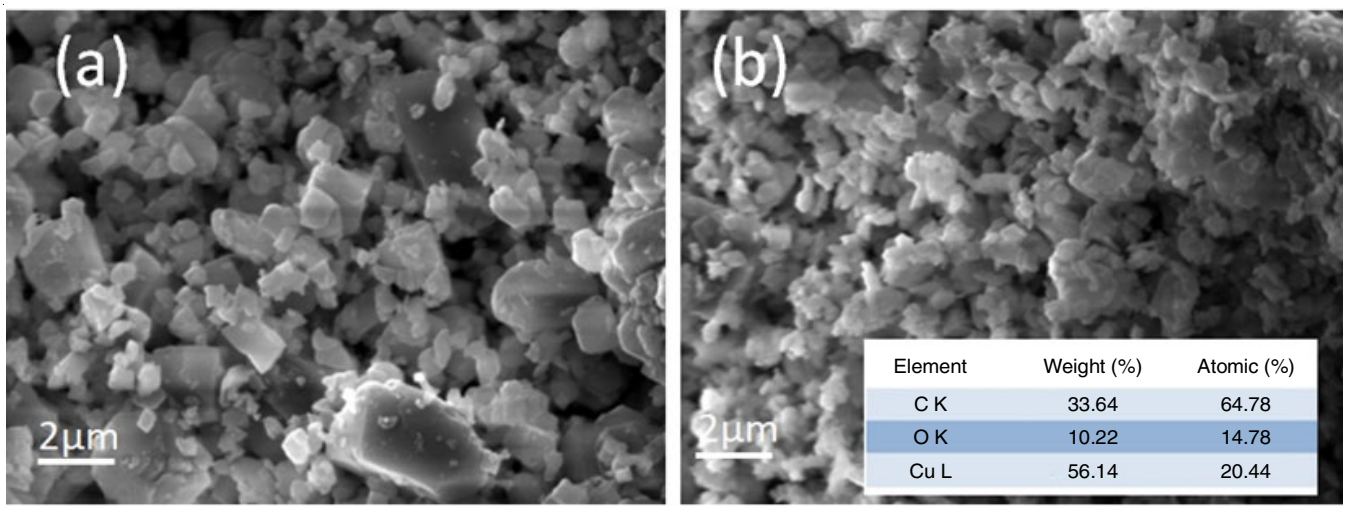

Fig. 3. FE-SEM images of (a) Cu-BDC and (b) C-Cu composite (inset shows elemental composition measured by SEM-EDX)

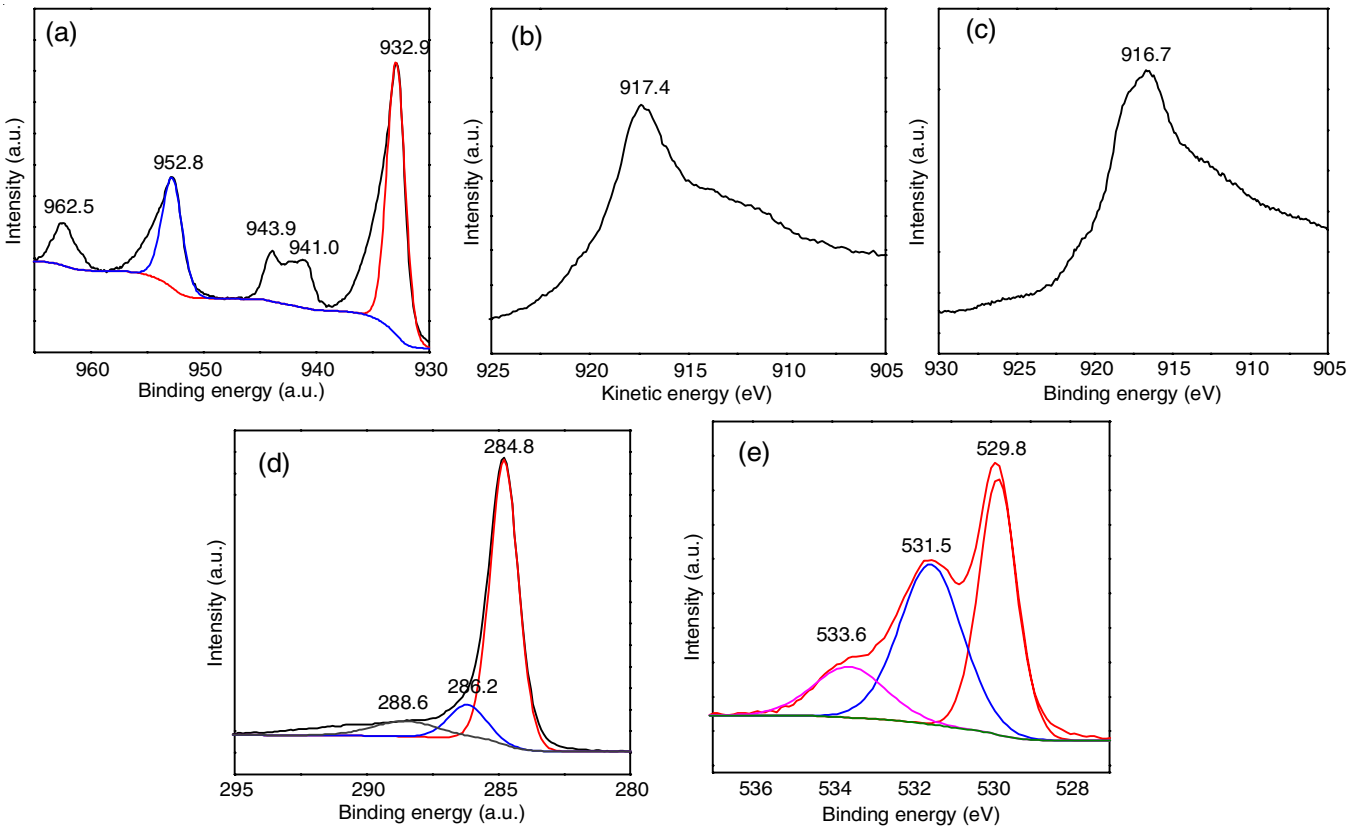

Fig. 4. XPS analysis of Cu-C composite: (a) Cu 2p; (b) CuLM2; (c) CuLM2 after two consecutive Ar etching; (d) C 1s; (e) O 1s

C=O (288.6 eV) [37]. On the other hand, the O1s scan (Fig. 4e) indicated the presence of Cu-O (529.8 eV) along with C=O (531.9 eV) and C-O (533.6) groups on the surface of the catalysts. Analysis of the deconvoluted XPS peaks of C1s and O1s of the catalyst confirmed the presence of carboxylic groups on the surface.

Catalytic reduction of *p*-nitrophenol: Fig. 5a shows the changes in the UV-vis spectra during the $NaBH_4$-assisted reduction of *p*-nitrophenol using Cu-C catalyst. Pure *p*-nitrophenol solution exhibited a distinctive UV- UV-absorbance peak at 317 nm, whereas the addition of $NaBH_4$ shifted the absorbance peak to 400 nm with a colour change from light yellow to bright yellow. This happened because of the transformation of *p*-nitrophenol to deprotonated *p*-nitrophenolate (NP^-) ions as the pH rises from 6 to 10 by the addition of $NaBH_4$ [38]. The solution was stable without the catalyst and even after 12 h, there was no discernible change in the absorbance intensity or peak position (400 nm).

Although $NaBH_4$ is a reducing agent with strong reduction potential, it was not effective in reducing *p*-nitrophenol without catalyst (Fig. 5b). However, it becomes highly reactive to reduce *p*-nitrophenol in the presence of solid catalyst [2,39]. To examine

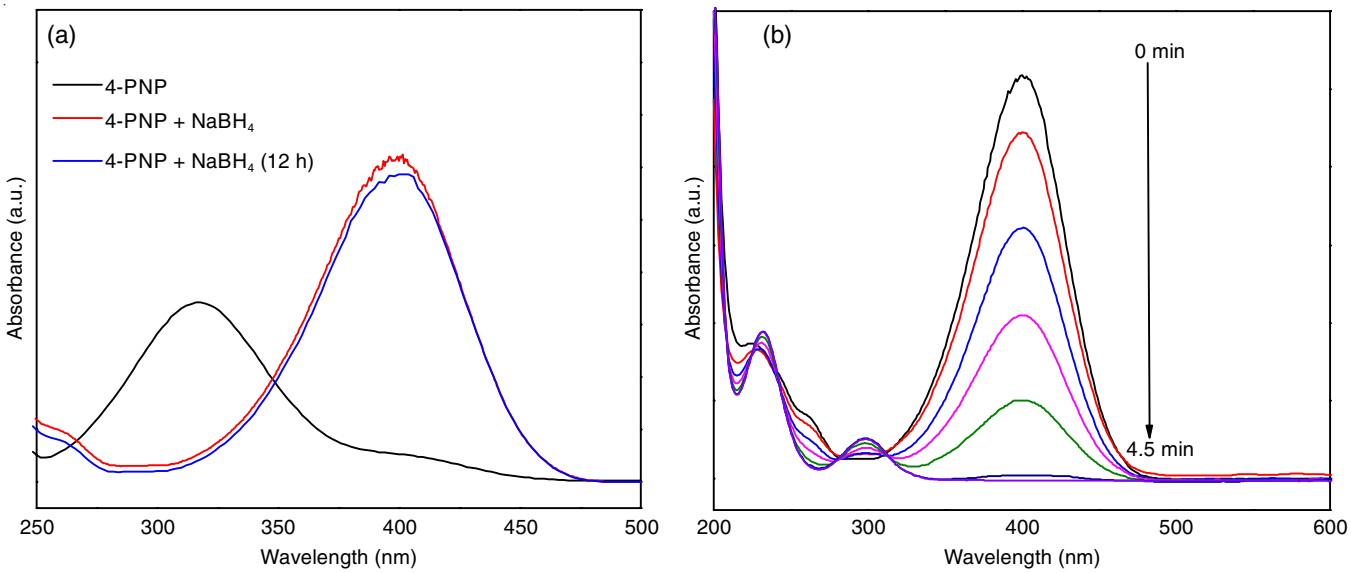

Fig. 5. (a) UV-vis spectrum of PNP before and after the addition of $NaBH_4$; (b) Changes of UV-vis spectrum during the reduction of PNP by 0.1 M $NaBH_4$ in the presence of Cu-C composites

the effect of the concentration of $NaBH_4$ on the reduction of *p*-nitrophenol, experiments were conducted at varying concentrations of $NaBH_4$. In these experiments, *p*-nitrophenol concentration was kept constant, while $NaBH_4$ concentrations were varied within the range of 0.1-0.3 M. Fig. 6 shows pseudo-first-order decays of *p*-nitrophenol catalyzed by Cu-C at varying $NaBH_4$ concentrations. The pseudo-first-order rate constants (k_{obs}) were found to be 0.441, 0.693, 2.16 and 2.27 min^{-1} in the presence of 0.1, 0.15, 0.2 and 0.3 M $NaBH_4$, respectively. The leveling-off effect of the *p*-nitrophenol reduction rate at > 0.2 M $NaBH_4$ is likely due to the saturation of $NaBH_4$ in the reaction media.

Fig. 7a compares the catalytic capabilities of Cu-C and CuO in mediating *p*-nitrophenol reduction at 0.2 $NaBH_4$. The Cu-C exhibited much higher catalytic activity than CuO, yielding an approximately 7-fold increase in the reaction rate (Fig. 7b). The enhanced catalytic activity of Cu-C over CuO might stem from the synergistic role of carbon in mediating electron transfer reactions to oxidize *p*-nitrophenol occurring on Cu catalyst surface [14]. Table-1 presents a comparison of the catalytic activity of Cu-C with previously reported catalysts used for *p*-nitrophenol reduction. It indicates that Cu-C composite has much higher catalytic capability than other noble metal catalysts such as Ag, Au, Pd, *etc.*

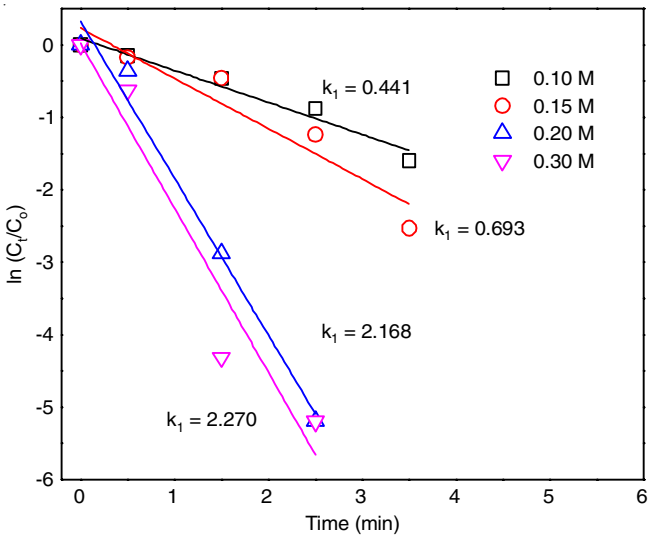

Fig. 6. Effect of the $NaBH_4$ concentration on catalytic reduction of PNP by Cu-C composite

TABLE-1
COMPARISON OF RATE CONSTANTS (k_{obs}) OF DIFFERENT CATALYSTS FOR THE REDUCTION OF PNP TO PAP

Catalyst	PNP conc. (mM)	$NaBH_4$ conc. (mM)	Amount of catalyst (mg)	Rate constant (min^{-1})	Rate activity parameter ($k' = k_{obs}/m$) (min^{-1} mg^{-1})	Ref.
Cu/MCM-41–24	0.05	0.15	3.00	6.54	2.17	[40]
Cu_2O@CMK-8	0.09	50	0.20	0.34	1.700	[41]
Cu/AC-600–1	0.10	12	1.00	0.78	0.780	[42]
Au@CeO_2 yolk-shell NPs	1.00	100	0.07	0.77	10.950	[43]
Fe_3O_4/SiO_2@PDA/Pd	3.00	300	2.00	4.51	2.250	[44]
Ag/g-C_3N_4/V_2O_5	10.00	500	0.05	0.37	7.400	[45]
Au/Fe_3O_4	10.00	100	2.00	0.63	0.320	[46]
Ag/SiO_2	0.22	3.2	0.31	1.07	3.450	[47]
Pd/GA/rGO	5.00	0.5	20.00	0.12	0.006	[48]
Cu-C	0.16	1.3	0.20	2.27	11.35	Present study

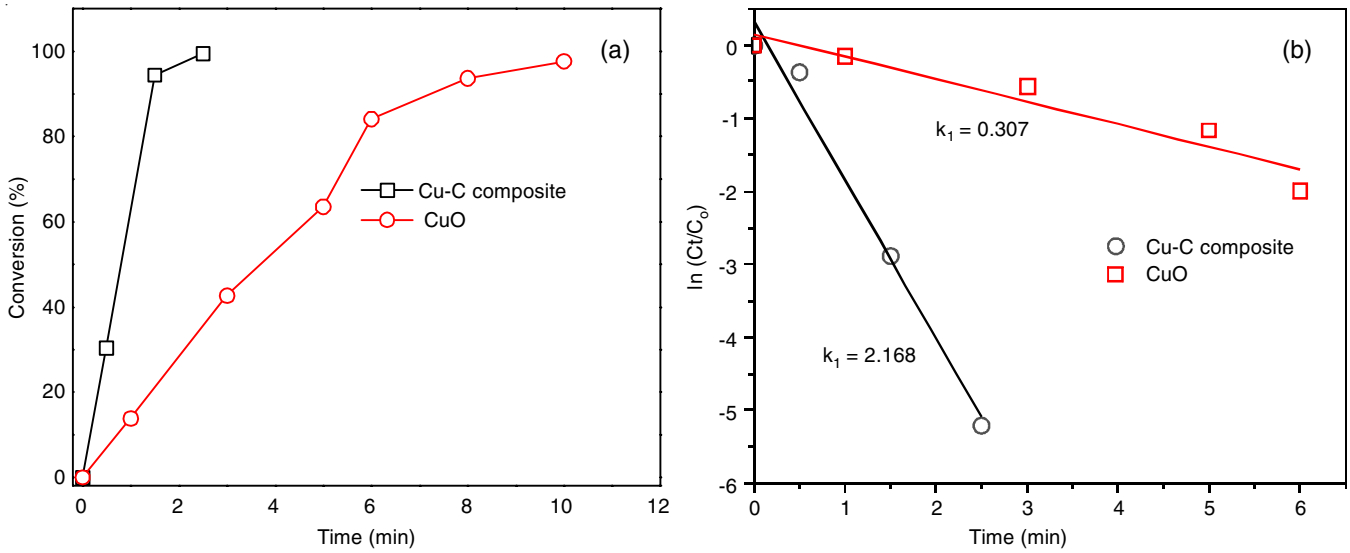

Fig. 7. (a) Catalytic conversion of PNP by Cu-C composite and CuO; (b) The relationship between $\ln(A_t/A_o)$ and reaction time (t) for the reduction of PNP in the presence of 0.2 M $NaBH_4$ by different catalysts

Plausible mechanisms: In the catalytic *p*-nitrophenol (PNP) removal process, the addition of $NaBH_4$ into an aqueous medium generates sodium cations (Na^+) and borohydride (BH_4^-) anions, which turns the solution basic [49]. When the pH of solution increases above the pK_a value of *p*-nitrophenol (7.1), deprotonation of *p*-nitrophenol occurs to generate NP^-. The standard reduction potential of *p*-nitrophenol ($E^o_{PNP/PAP}$) and $NaBH_4$ ($E^o_{H_3BO_3/BH_4^-}$) are -0.76 and -1.33 V, respectively [49]. Although the redox reaction of PNP/$NaBH_4$ pair is thermodynamically feasible based on their potential difference, the process is sterically hindered because of electrostatic repulsion between the anions, NP^- and BH_4^-. Under this condition, the possible reduction mechanism can be depicted by the following steps: (i) adsorption of NP^- and BH_4^- ions onto the surface of the catalyst; (ii) generation of hydrogen from the reduction of water, followed by hydride generation on the catalyst surface; (iii) reduction of *p*-nitrophenol to *p*-aminophenol (PAP); and (iv) desorption of *p*-aminophenol from the catalyst. A $NaBH_4$-associated catalytic reduction *p*-nitrophenol can be well described by the Langmuir-Hinshel-wood mechanism [50].

The generation of hydrogen proceeds *via* dissociative adsorption of BH_4^- and H_2O on the catalyst's surface. Then, BH_4^- undergoes four consecutive hydrolyses where each BH_4^- reacts with an equal amount of adsorbed H_2O to generate one H_2 (Fig. 8). The generated H_2 interacts with Cu-C on the surface of catalyst to produce metal/metal oxide-hydride complexes [51]. These hydride complexes generate reactive hydrides (H^-) that react with NP^- to cause N-O single-bond cleavage. Another breaking of N-O proceeds *via* the reaction of additional H^- to form 4-hydroxyl-aminophenol intermediate. Further attack of H^- towards these intermediate finally results in the formation of *p*-aminophenol [51]. After complete reduction, the N atom in $-NO_2$ becomes electron-rich and promotes rapid desorption from the surface of catalyst [52]. Previous studies demonstrated that Cu or Cu oxides, including CuO or Cu_2O, show good catalytic activity in the $NaBH_4$-mediated catalytic reduction of nitrophenols, which is in good agreement with this work [53]. Furthermore, carbon support possesses different functional groups that can interact with *p*-nitrophenol *via* several interactions, including hydrogen bonding, π-π stacking, *etc.* These phenomena can accelerate the adsorption of *p*-nitrophenol into the surface of catalyst.

Reusability studies: The reusability of catalyst of a critical material characteristic determines the actual applicability of the material as it is closely related to cost and secondary pollution by the catalyst. To address this issue, the reusability of Cu-C was analyzed. As shown in Fig. 9, Cu-C showed very robust reusability, keeping more than 96% conversion up to the fourth cycle. However, the time needed to complete each cycle increased from 2.5 min in the first cycle to 5 min in the fourth cycle, showing a slight decrease in the catalytic efficiency. The decrease in catalytic efficiency might be attributed to the leaching of a small number of active species, along with the partial blocking of the active sites.

Conclusion

A Cu-carbon composite was synthesized *via* one-step carbonization of a Cu-based metal-organic framework (MOF) at 600 ºC under an inert atmosphere. Upon heating, the MOF structure was destroyed and XRD confirmed the generation of new CuO and Cu phases. The SEM images indicated the reduction of particle size after calcination. The presence of Cu^{2+} and a small amount of Cu^+ was confirmed *via* XPS analysis. *p*-Nitrophenol reduction kinetics depended on the $NaBH_4$ concentration up to a limited level. The Cu-C completely reduced 0.16 mM *p*-nitrophenol within 2.5 min, which is far better than commercial CuO. In presence of $NaBH_4$, catalytic reduction of *p*-nitrophenol by Cu-C can be well defined by the Langmuir–Hinshelwood mechanism. Besides, it shows good reusability up to four sequential cycles for reducing *p*-nitrophenol to *p*-aminophenol with only a small loss of catalytic ability. Consequently, the synthesized Cu-C displayed their potential in $NaBH_4$-assisted catalysis of *p*-nitrophenol.

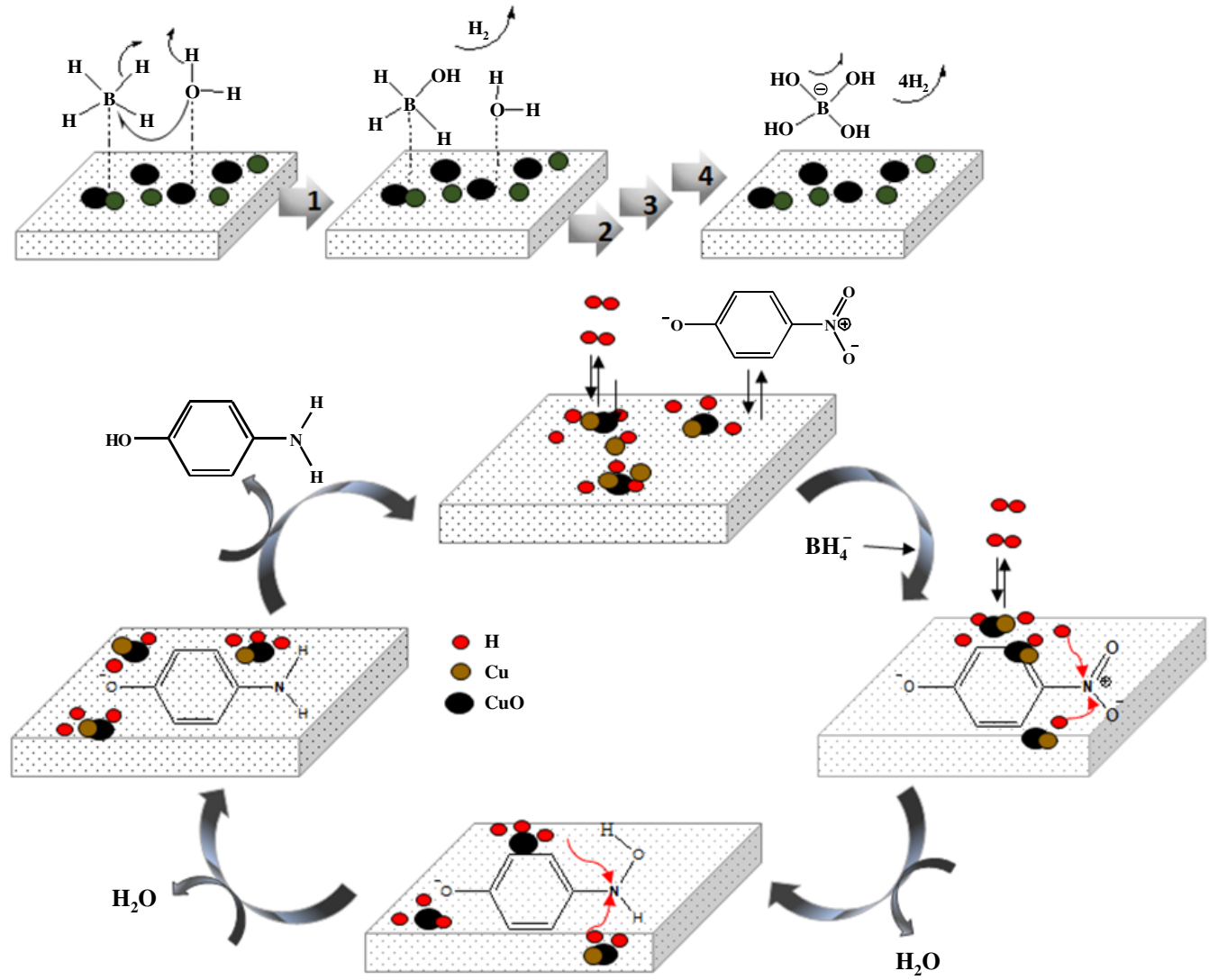

Fig. 8. Plausible mechanism for the conversion of *p*-nitrophenol (PNP) to *p*-aminophenol (PAP) over Cu-C composites in the presence of $NaBH_4$

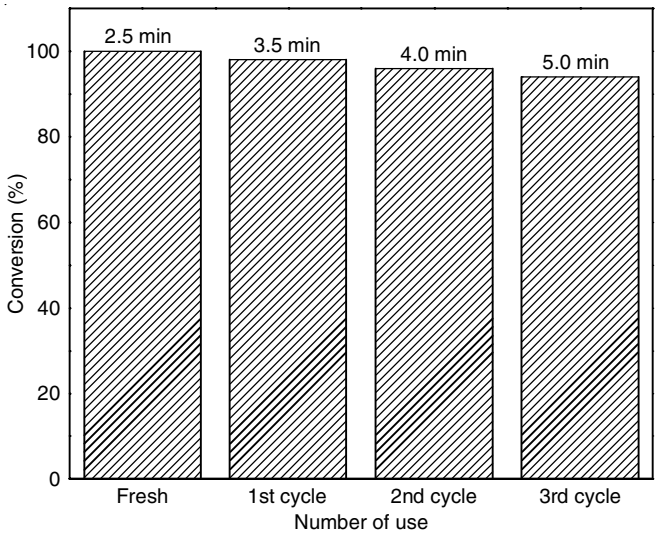

Fig. 9. Reusability of Cu-C composite during the reduction of *p*-nitrophenol (PNP) in the presence of 0.2 M $NaBH_4$; the text over each bar represents the time required to accomplish each complete cycle for the reduction of *p*-nitrophenol (PNP) by Cu-C composite

ACKNOWLEDGEMENTS

This work was financially supported by East West University Centre of Research and Training (EWUCRT), Dhaka, Bangladesh.

CONFLICT OF INTEREST

The authors declare that there is no conflict of interests regarding the publication of this article.

REFERENCES

1. J. Xia, G. He, L. Zhang, X. Sun and X. Wang, *Appl. Catal. B*, **180**, 408 (2016); https://doi.org/10.1016/j.apcatb.2015.06.043
2. Z. Hasan, D.W. Cho, C.M. Chon, K. Yoon and H. Song, *Chem. Eng. J.*, **298**, 183 (2016); https://doi.org/10.1016/j.cej.2016.04.029
3. N. Sahiner, S. Yildiz and H. Al-Lohedan, *Appl. Catal. B*, **166–167**, 145 (2015); https://doi.org/10.1016/j.apcatb.2014.11.027
4. V. Uberoi and S.K. Bhattacharya, *Water Environ. Res.*, **69**, 146 (1997); https://doi.org/10.2175/106143097X125290

5. Y. Zheng, J. Shu and Z. Wang, *Mater. Lett.*, **158**, 339 (2015); https://doi.org/10.1016/j.matlet.2015.06.033
6. J. Xing, Q. Peng, W. Zhong, Y. Zhang, X. Wang and K. Liu, *J. Water Process Eng.*, **51**, 103403 (2023); https://doi.org/10.1016/j.jwpe.2022.103403
7. J. Feng, L. Fang, Y. Zhang and H. Zhao, *Mater. Sci. Semicond. Process.*, **163**, 107537 (2023); https://doi.org/10.1016/j.mssp.2023.107537
8. H. Zheng, W. Guo, S. Li, Y. Chen, Q. Wu, X. Feng, R. Yin, S.H. Ho, N. Ren and J.S. Chang, *Bioresour. Technol.*, **244**, 1456 (2017); https://doi.org/10.1016/j.biortech.2017.05.025
9. G. Chu, W. Wang, Y. Dou, K. Sun, W. Qin, Z. Wang and Y. Si, *Sci. Total Environ.*, **900**, 165797 (2023); https://doi.org/10.1016/j.scitotenv.2023.165797
10. A. Tang, M. Long and Z. He, *Electrochim. Acta*, **146**, 346 (2014); https://doi.org/10.1016/j.electacta.2014.09.027
11. H. Cheng, N. Han, Z. Bai, Z. Li, W. Xu and S. Xiao, *Surf. Interfaces*, **39**, 102929 (2023); https://doi.org/10.1016/j.surfin.2023.102929
12. R. Hu, R. Xu, Z. Wang, J. Wang and S. Zhou, *Chem. Eng. J.*, **471**, 144780 (2023); https://doi.org/10.1016/j.cej.2023.144780
13. M. Kubo, T. Matsumoto and M. Shimada, *Adv. Powder Technol.*, **33**, 103701 (2022); https://doi.org/10.1016/j.apt.2022.103701
14. A. Khan, Z. Liao, Y. Liu, A. Jawad, J. Ifthikar and Z. Chen, *J. Hazard. Mater.*, **329**, 262 (2017); https://doi.org/10.1016/j.jhazmat.2017.01.029
15. D. Patil, J. Manjanna, S. Chikkamath, V. Uppar and M. Chougala, *J. Hazard. Mater. Adv.*, **4**, 100032 (2021); https://doi.org/10.1016/j.hazadv.2021.100032
16. L.A. Ramirez, M. Dennehy and M. Alvarez, *Catal. Commun.*, **181**, 106723 (2023); https://doi.org/10.1016/j.catcom.2023.106723
17. X. Xu, K. Jia, S. Chen, D. Lang, C. Yang, L. Wang, R. Wu, W. Wang and J. Wang, *J. Environ. Chem. Eng.*, **9**, 105505 (2021); https://doi.org/10.1016/j.jece.2021.105505
18. A. Šuligoj, I. Trendafilova, K. Maver, A. Pintar, A. Ristiæ, G. Dra•ic, W.H.M. Abdelraheem, Z. Jaglièiæ, I. Arèon, N.Z. Logar, D.D. Dionysiou and N. Novak Tušar, *J. Environ. Chem. Eng.*, **11**, 110369 (2023); https://doi.org/10.1016/j.jece.2023.110369
19. H.C. Zhou, J.R. Long and O.M. Yaghi, *Chem. Rev.*, **112**, 673 (2012); https://doi.org/10.1021/cr300014x
20. Q. Wang and D. Astruc, *Chem. Rev.*, **120**, 1438 (2020); https://doi.org/10.1021/acs.chemrev.9b00223
21. Z. Hasan and S.H. Jhung, *J. Hazard. Mater.*, **283**, 329 (2015); https://doi.org/10.1016/j.jhazmat.2014.09.046
22. V. Snowlin, H.J. Prabu, A.F. Sahayaraj, I. Johnson, E. Thaninayagam, R.R. Gopi, J. Salamon and A. Simi, *J. Inorg. Organomet. Polym. Mater.*, (2023); https://doi.org/10.1007/s10904-023-02823-5
23. T. Jia, Y. Gu and F. Li, *J. Environ. Chem. Eng.*, **10**, 108300 (2022); https://doi.org/10.1016/j.jece.2022.108300
24. N.A. Khan and S.H. Jhung, *J. Hazard. Mater.*, **237–238**, 180 (2012); https://doi.org/10.1016/j.jhazmat.2012.08.025
25. A. Bavykina, N. Kolobov, I.S. Khan, J.A. Bau, A. Ramirez and J. Gascon, *Chem. Rev.*, **120**, 8468 (2020); https://doi.org/10.1021/acs.chemrev.9b00685
26. C.S. Gujja and S.D. Pawar, *J. Inorg. Organomet. Polym. Mater.*, **33**, 2636 (2023); https://doi.org/10.1007/s10904-023-02669-x
27. W. Chaikittisilp, K. Ariga and Y. Yamauchi, *J. Mater. Chem. A Mater. Energy Sustain.*, **1**, 14 (2013); https://doi.org/10.1039/C2TA00278G
28. Y. Wang, J. Xu, X. Lin, B. Wang, Z. Zhang, Y. Xu and Y. Suo, *J. Solid State Chem.*, **322**, 123984 (2023); https://doi.org/10.1016/j.jssc.2023.123984
29. A. Deng, Y. Yin, Y. Liu, Y. Xu, H. He, S. Yang, Q. Qin, D. Sun and S. Li, *Sep. Purif. Technol.*, **318**, 123998 (2023); https://doi.org/10.1016/j.seppur.2023.123998
30. D. Zhu, L. Wang, W. Yu and H. Xie, *Sci. Rep.*, **8**, 5282 (2018); https://doi.org/10.1038/s41598-018-23174-z
31. G. Zhang, B. Xu, H. Chong, W. Wei, C. Wang and G. Wang, *RSC Adv.*, **9**, 14016 (2019); https://doi.org/10.1039/C9RA01385G
32. R.S. Salama, S.E. Samra, A.I. Ahmed, S.A. El-Hakam, S.E. Samra and S.M. El-Dafrawy, *Int. J. Med. Chem.*, **10**, 195 (2018); https://www.researchgate.net/publication/327097878
33. A.C. Elder, A.B. Aleksandrov, S. Nair and T.M. Orlando, *Langmuir*, **33**, 10153 (2017); https://doi.org/10.1021/acs.langmuir.7b01987
34. B. Nageswara Rao, P. Tirupathi Rao, S.E. Basha, D.S.L. Prasanna, K. Samatha and R.K. Ramachandra, *Mater. Chem. Phys.*, **308**, 128174 (2023); https://doi.org/10.1016/j.matchemphys.2023.128174
35. S. Poulston, P.M. Parlett, P. Stone and M. Bowker, *Surf. Interface Anal.*, **24**, 811 (1996); https://doi.org/10.1002/(SICI)1096-9918(199611)24:12<811::AID-SIA191>3.0.CO;2-Z
36. T. Aditya, J. Jana, N.K. Singh, A. Pal and T. Pal, *ACS Omega*, **2**, 1968 (2017); https://doi.org/10.1021/acsomega.6b00447
37. A. Siri, A. Wongrueng, P. Rakruam and P. Punyapalakul, *J. Environ. Chem. Eng.*, **11**, 110464 (2023); https://doi.org/10.1016/j.jece.2023.110464
38. K. Naseem, R. Begum, W. Wu, A. Irfan, J. Nisar, M. Azam and Z.H. Farooqi, *Int. J. Environ. Sci. Technol.*, **18**, 1809 (2021); https://doi.org/10.1007/s13762-020-02913-8
39. M. Liu, B. Niu, H. Guo, S. Ying and Z. Chen, *Inorg. Chem. Commun.*, **130**, 108687 (2021); https://doi.org/10.1016/j.inoche.2021.108687
40. S. Schlichter, M. Rocha, A.F. Peixoto, J. Pires, C. Freire and M. Alvarez, *Polyhedron*, **150**, 69 (2018); https://doi.org/10.1016/j.poly.2018.04.037
41. P.C. Rath, D. Saikia, M. Mishra and H.M. Kao, *Appl. Surf. Sci.*, **427**, 1217 (2018); https://doi.org/10.1016/j.apsusc.2017.08.097
42. S. Wang, S. Gao, Y. Tang, L. Wang, D. Jia and L. Liu, *J. Solid State Chem.*, **260**, 117 (2018); https://doi.org/10.1016/j.jssc.2018.01.025
43. C.M. Fan, L.F. Zhang, S.S. Wang, D.H. Wang, L.Q. Lu and A.W. Xu, *Nanoscale*, **4**, 6835 (2012); https://doi.org/10.1039/c2nr31713c
44. E. Farzad and H. Veisi, *J. Ind. Eng. Chem.*, **60**, 114 (2018); https://doi.org/10.1016/j.jiec.2017.10.017
45. H.S. EL-Sheshtawy, H.M. El-Hosainy, K.R. Shoueir, I.M. El-Mehasseb and M. El-Kemary, *Appl. Surf. Sci.*, **467-468**, 268 (2019); https://doi.org/10.1016/j.apsusc.2018.10.109
46. S. Bae, S. Gim, H. Kim and K. Hanna, *Appl. Catal. B*, **182**, 541 (2016); https://doi.org/10.1016/j.apcatb.2015.10.006
47. Y. Shi, X.L. Zhang, G. Feng, X. Chen and Z.H. Lu, *Ceram. Int.*, **41**, 14660 (2015); https://doi.org/10.1016/j.ceramint.2015.07.188
48. A.T.E. Vilian, S.R. Choe, K. Giribabu, S.C. Jang, C. Roh, Y.S. Huh and Y.K. Han, *J. Hazard. Mater.*, **333**, 54 (2017); https://doi.org/10.1016/j.jhazmat.2017.03.015
49. T. Aditya, A. Pal and T. Pal, *Chem. Commun.*, **51**, 9410 (2015); https://doi.org/10.1039/C5CC01131K
50. J. Andrieux, U.B. Demirci and P. Miele, *Catal. Today*, **170**, 13 (2011); https://doi.org/10.1016/j.cattod.2011.01.019
51. A. Verma, P. Anand, S. Kumar and Y.P. Fu, *Appl. Surf. Sci.*, **578**, 151795 (2022); https://doi.org/10.1016/j.apsusc.2021.151795
52. X. Sun, P. He, Z. Gao, Y. Liao, S. Weng, Z. Zhao, H. Song and Z. Zhao, *J. Colloid Interface Sci.*, **553**, 1 (2019); https://doi.org/10.1016/j.jcis.2019.06.004
53. K. Sahu, B. Satpati, R. Singhal and S. Mohapatra, *J. Phys. Chem. Solids*, **136**, 109143 (2020); https://doi.org/10.1016/j.jpcs.2019.109143